Precise Control of Lamellar Thickness in Highly Oriented Regioregular Poly(3-Hexylthiophene) Thin Films Prepared by High-Temperature Rubbing: Correlations with Optical Properties and Charge Transport

Amer Hamidi-Sakr, Laure Biniek, Sadiara Fall, Martin Brinkmann

Precise control of lamellar thickness in highly oriented regioregular poly(3-hexylthiophene) thin films prepared by high temperature rubbing : correlations with optical properties and charge transport

Amer Sakr-Hamidi[1], Laure Biniek[1], Sadiara Fall[2] and Martin Brinkmann[1]

(1) Institut Charles Sadron, CNRS – Université de Strasbourg, 23 rue du Loess, 67034 Strasbourg, France

(2) ICUBE, MaCEPV, Université de Strasbourg, 23 rue du Loess, 67037, Strasbourg, France

* Corresponding author : e-mail : martin.brinkmann@ics-cnrs.unistra.fr

Figure for Title of content

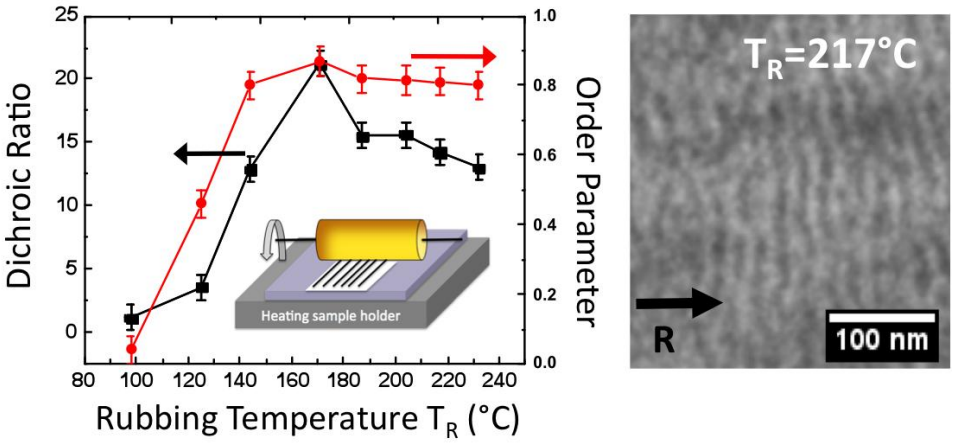

Precise control of orientation and crystallinity is achieved in regioregular poly(3-hexylthiophene) thin films by using high temperature rubbing, a fast and effective alignment method. Uniquely, the exciton coupling in P3HT is correlated to the length of the planarized chain segments in the crystals. The evolution of charge transport *versus* rubbing temperature is correlated to the crystal orientation and film nanomorphology.

Abstract

Precise control of orientation and crystallinity is achieved in regioregular poly(3-hexylthiophene) thin films by using high temperature rubbing, a fast and effective alignment method. Rubbing P3HT films at temperatures $T_R \geq 144°C$ generates highly oriented crystalline films with a periodic lamellar morphology with dichroic ratio reaching 25. The crystallinity and the average crystal size along the chain axis direction, l_c, were determined by High Resolution Transmission Electron Microscopy and Differential Scanning Calorimetry. The inverse of the lamellar period l scales with the supercooling and can accordingly be controlled by the rubbing temperature T_R. Uniquely, the observed exciton coupling in P3HT crystals is correlated to the length of the average planarized chain segments l_c in the crystals. The high alignment and crystallinity observed for $T_R>200°C$ cannot translate to high hole mobilities parallel to the rubbing because of the adverse effect of amorphous zones interrupting charge transport between crystalline lamellae. Although tie chains bridge successive P3HT crystals through amorphous zones, their twisted conformation restrains inter-lamellar charge transport. The evolution of charge transport anisotropy is correlated to the evolution of the dominant contact plane from mainly face-on ($T_R \leq 100°C$) to edge-on ($T_R \geq 170°C$).

1. Introduction.

Semi-crystalline polymer semi-conductors are popular and key materials in the fabrication of low cost electronic devices. Mastering their charge transport properties in thin films is challenging as it is a complex multi-scale physical process that depends closely on the level of order achieved at multiple length scales.[1] At the molecular scale, intra-chain transport is favored by the chain planarization which can be enforced by crystallization for polymers such as poly(alkylthiophene)s (P3HT or pBTTT).[2,3] At the mesoscale, charge transport is further affected by the intrinsic semi-crystalline morphology of SCPs i.e. the fact that crystalline regions coexist with amorphous zones in the polymer.[4,5] Charges must therefore cross the boundaries between highly conductive crystalline and poorly conductive amorphous domains in the films and this is why controlling the nanomorphology of semi-conducting polymers (SCPs) is an important issue.[6] In this regard, molecular weight was found to influence strongly charge transport. This is because, depending on the average contour length of the chains, so-called tie-chains can link crystalline domains through the amorphous interlamellar zones and impact the charge transport in thin films.[7] Therefore, it is important to develop processing methods to control precisely the relative proportions of amorphous and crystalline fractions in SCPs i.e. to control the crystal size distribution and orientation in a thin film. In this perspective, the role of molecular weight is essential as it fixes the average contour length l_{chain} with respect to the average crystal size along the chain direction l_c. Furthermore, charge transport is highly anisotropic in systems such as P3HT, being most effective along the chain axis direction (c axis) and the π-stacking direction (b axis) and poor along the insulating alkyl side chains (a axis).[8,9] Accordingly, a comprehensive approach to charge transport in SCPs requires to control both orientation and crystal dimensions in thin films.

The role of structural perfection on charge transport was recently addressed by Salleo and coworkers from the perspective of paracrystallinity along the π-stacking direction.[1] Paracrystallinity is a measure of the lattice disorder obtained from the careful analysis of X-ray diffraction peaks. Although correlations were observed for various polymers between charge mobility and paracrystallinity, it is surprising that no direct correlation between crystalline order along the chain direction and charge mobility was established so far. One of the reasons for this is that the precise control of both orientation and crystallite size is usually difficult to achieve in SCPs films. Moreover, crystal dimensions along the chain direction are virtually impossible to extract from classical Grazing Incidence X-ray diffraction data on unoriented films given the poor intensities of the 0 0 l reflections. But there exist means to align SCPs and thus enhance order along the chain direction, to cite but a few: nanoimprint lithography,[10] epitaxy[11], flow coating,[12] strain orientation,[13] nanostructured confinement[14] and use of nanogrooved alignment layers.[15]

One of the reasons for the rather low crystallinity in SCPs is their poor ability to nucleate intrinsically, especially from the melt, because of the entanglements between rigid chains that can hardly disentangle, even at elevated temperatures. In solution, control of nucleation and growth seems more straightforward and in the case of P3HT, it was demonstrated by Reiter and Ludwigs, that the density of nucleation of P3HT spherulites can be tuned by solvent vapor annealing.[16] Emerick et al.[17] as well as Stingelin et al.[18] showed that nucleation agents can be used either in solution or in the melt to favor crystallization of SCPs. Alternatively, Stingelin et al. proposed to use crystallization under pressure to promote extended chain crystallization of P3HT but with limited success.[18]

Another approach to enhance the nucleation of polymer crystals consists in aligning the chains either by epitaxial interactions with a substrate or by using shear stress.[19] High crystallinity and orientation of P3HT were obtained by epitaxial crystallization whereby a

crystalline substrate serves as a template to orient polymer chains acting as seeds for the subsequent growth.[5,11] Substrates of oriented polyethylene,[20] 1,3,5-trichlorobenzene,[6, 21] or carbon nanotubes[22] where successfully used to nucleate and align P3HT crystals from solution.

As an alternative, rubbing was proposed as an efficient method to align SCPs. Rubbing is a well-known technique to prepare alignment layers of polyimides further used to orient liquid crystals.[23] Typically, a cylinder covered with a velvet cloth, rotates over a polymer film whereby surface alignment of polymer chains is induced.[18, 24-26] When applied to SCPs, it turned out that both temperature and molecular weight of the polymer are two key parameters controlling the level of alignment.[25,27,28] At high rubbing temperatures, polymer chains can disentangle (when the alkyl side chains of the SCPs are in a molten state) and align parallel to the rubbing direction. Bundles of aligned chains can then serve as seeds for the oriented crystallization of the SCPs.

This work extends our previous studies on high-T rubbing by investigating the range of very high rubbing temperatures above 200°C and close to the melting of P3HT (240°C). To our surprise, it is observed that a solid state treatment such as high-T rubbing can generate very high levels of order in thin films that could usually only be observed in P3HT films processed from solution, not from the melt. Herein, precise control over lamellar periods is obtained for the first time by high-T rubbing of P3HT. Correlations between crystal dimension and the excitonic band width could be established. Moreover, the evolution of charge transport anisotropy with T_R is correlated to the change of preferred contact plane of P3HT crystals in the oriented films.

2. Results and discussion.

2.1. Orientation and lamellar morphology at high rubbing temperature.

a) Alignment versus rubbing temperature.

Improved orientation of P3HT at temperatures up to 180°C was recently demonstrated.[27,28] Hereafter, it is shown that using even higher temperatures close to the melting of the polymer can further modify crystallinity in the P3HT films to a level close to that usually observed in films prepared from solutions in organic solvents. Figure 1.a and b depicts the changes in the UV-vis spectra of rubbed P3HT at various temperatures whereas Figure 1.c shows the T_R-dependence of the dichroic ratio DR and the 3D order parameter S defined as S=(DR-1)/(DR+2). The change in the level of orientation is clear from the UV-vis spectra and the T_R-dependence of DR and S. It shows that a maximum of orientation is achieved when T_R reaches ~171°C. Beyond this temperature, S tends to decrease slightly and levels at a value close to 0.8. Importantly, for $T_R \geq 171$°C, the absorption spectrum for $\perp$ orientation does not show any vibronic structure and is peaked at 500 nm. As a matter of fact, for a polarization perpendicular to R, the film's color is orange, i.e. similar to the absorption of coiled P3HT in solution but it is red-shifted by 57 nm and significantly broader (See Figure S1). Such a spectrum indicates that the chains in the amorphous zones do not have a planar conformation but contain twists between successive thiophene units that break π-conjugation along the chain, leading to a large distribution of conjugation lengths. Moreover, the spectrum is close to that obtained in spin-coated films of the hexane fraction of P3HT (M_n=5.6kDa) showing a poor crystallinity.[29] This suggests that the P3HT chains in the amorphous zones could be composed in majority of small M_w fractions i.e. those chains that are too short to crystallize at the rubbing temperatures (GPC results in Figure S2 indicate the presence of short chains in the samples). In other words, this would imply some type of M_w-fractionation during crystallization, the smaller P3HT chains being rejected to the

amorphous interlamellar zones. These effects are somehow similar to that observed for crystallization of P3HT nanofibrils in solution in anisole.[30] Indeed, upon crystallization of P3HT nanofibrils in anisole, the low–M_w fractions of P3HT are left in solution.

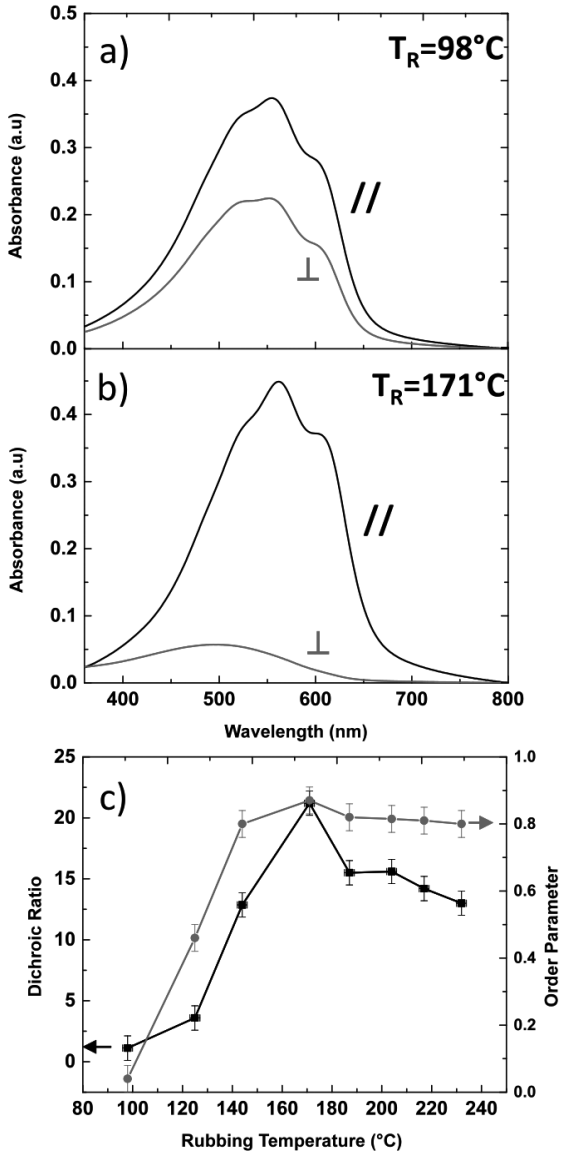

Figure1. Polarized UV-Vis spectra of oriented P3HT films (M_w=50 kDa) rubbed at T_R=98°C (a) and 171°C (b). Figure 1.c depicts the dependence of the dichroic ratio DR at 610 nm (full squares) and of the 3D order parameter (full grey circles) defined as (DR-1)/(DR+2) as a function of the rubbing temperature.

Despite the decrease in overall orientation for T_R> 171°C, the intensity of the 0-0 component in the vibronic structure of the spectrum still increasing with T_R. The spectrum observed in films rubbed at T_R=217°C is similar to that observed in P3HT films cast from high boiling point solvents indicating that crystalline order is still improving. The vibronic structure in the absorption of such rubbed films is significantly more pronounced when compared to that observed for P3HT films oriented by strain alignment, suggesting superior crystallinity in high-T rubbed P3HT films.[13] As shown hereafter, this trend is further supported by TEM in bright-field (BF-TEM) and diffraction.

b) Periodic lamellar structure.

P3HT is known to be a semi-crystalline polymer and its structure in films oriented by epitaxy was shown to consist of a periodic alternation of crystalline lamellae and amorphous interlamellar zones.[5] As seen in Figure 2, all the films rubbed at T_R≥144°C exhibit a similar periodic lamellar morphology in BF whereas for T_R≤125°C, no such morphology can be evidenced. Moreover, the contrast in the BF images between crystalline and amorphous domains tends to increase with T_R. Figure 2 depicts the evolution of the lamellar structure in rubbed films as a function of T_R whereas the plot in Figure 2.e shows the T_R-dependence of the lamellar period *l* extracted from the fast Fourier transforms. The lamellar period *l* increases with T_R, typically from 13 nm at 144°C to 26 nm at 217°C. The latter value is close to that observed in the semi-crystalline films of P3HT prepared by directional epitaxial crystallization.[5]

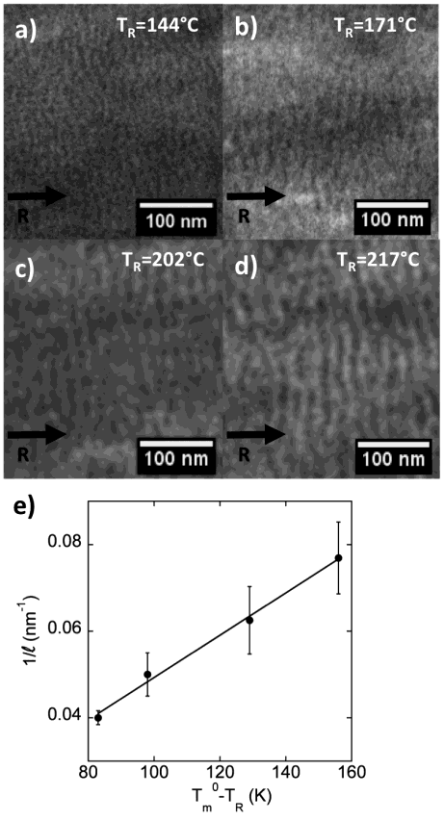

Figure 2. (a-d) TEM BF images of the lamellar morphologies in oriented P3HT films prepared by rubbing at different temperatures T_R. (e) shows the variation of the inverse of the lamellar period *l* extracted from the fast Fourier Transforms of the TEM BF images as a function of the supercooling where T_m^0 is the melting temperature of an infinite-sized P3HT crystal. The continuous line is the result of a fit yielding T_m^0=301±6°C.

For classical polymers such as polyethylene, the inverse of the lamellar period *l* is expected to scale with the supercooling following the relation $l^{-1} \propto (T_m^0 - T_R)$ where T_m^0 is the melting temperature of an infinite size crystal and T_c is the crystallization temperature.[31, 32]

As seen in Figure 2.e, this relation is indeed verified for the films of P3HT and the fit yields a value T_m^0=301°C±6°C. This value is found in excellent agreement with the

value of 300°C extracted from Hoffman-Weeks plots by Malik and Nandi [33] and the value of 298°C obtained by Koch et al. from the extrapolation of the melting temperature of a set of oligo-P3HTs,[34] but it is above the value of 272±6°C reported by Snyder et al.[35] While such an evolution of lamellar period with crystallization temperature is well known for classical polyolefins such as polyethylene[32], it is the first time that it is observed for a SCP such as P3HT.

Therefore, high-T rubbing is a unique method that allows to fine tune the lamellar period in semi-crystalline films of SCPs such as P3HT by adjusting the rubbing temperature. This is possible since the nucleation of crystalline domains, often difficult for such rigid polymers, is induced by mechanical rubbing at a sufficiently high temperature that allows P3HT to crystallize in the form of folded chain lamellae ultimately forming a regular lamellar semicrystalline morphology. Such a periodic lamellar morphology, also observed in epitaxied films, is different from the one found in cast and spin-coated films that consist of nanofibrils formed in solution under conditions that are far from equilibrium.

c) Electron diffraction.

Electron diffraction further evidences clear and remarkable structural variations in the rubbed films. Figure 3 shows the characteristic ED patterns versus T_R. As noted in our original work on rubbing of P3HT at room temperature, no orientation of P3HT (48 kDa) is observed at T_R=25°C. The ED pattern consists of an intense 0 2 0 Scherrer ring implying *edge-on* P3HT domains with random in-plane orientation.[36] For 98°C≤T_R≤144°C, a set of equatorial h 0 0 reflections characteristic of *face-on* P3HT domains replaces progressively the 0 2 0 Scherrer ring associated with the non aligned *edge-on* P3HT domains. For all the films prepared at T_R≤144°C, no well-defined 0 0 2 is

observed. Therefore, the structure of these films resembles a highly strained smectic-like phase with the thiophene backbones oriented along the rubbing direction R but without well-defined translational order along the chain direction c_{P3HT} between π-stacked polythiophene chains.[25]

A remarkable structural change takes place for $T_R \geq 171°C$. Beside the equatorial h 0 0 reflections, the ED patterns show several 0 k 2 reflections. For T_R = 217°C, the 0 0 2 reflection becomes quite intense and sharp. More generally, the ED patterns show numerous mixed indexes reflections up to q= 1.3 $Å^{-1}$ which could not be observed previously in oriented film (M_w=20 kDa) prepared by directional crystallization (see Figure 3.e). This indicates a very high level of crystalline order in P3HT films rubbed at 217°C, especially along the chain direction $\mathbf{c_{P3HT}}$. It also implies 3D order in the side chain packing. The enhanced sharpness of the 0 0 2 reflection along the meridian indicates larger crystals along c_{P3HT} which is fully consistent with the larger lamellar periods seen in BF. Moreover, for T_R=217°C, 0 2 *l* reflections appear on the equator beside the h 0 0 reflections (h=1-3), indicating that the films consist of aligned crystals (c_{P3HT}//R) with *face-on* and *edge-on* orientations on the substrate. However, for T_R=217°C, the films consist of a majority of aligned *edge-on* domains, as inferred from the strong intensity of the 0 2 0 equatorial reflection. The comparison of the 217°C ED pattern with the calculated fiber pattern (using the structure of form I by Kayunkid et al. [37]) in Figure 3.f indicates that i) the films rubbed at 217°C have the characteristic form I crystal structure and ii) that they do not show a perfect fiber symmetry as can be inferred from the absence of certain h k 1 reflections.

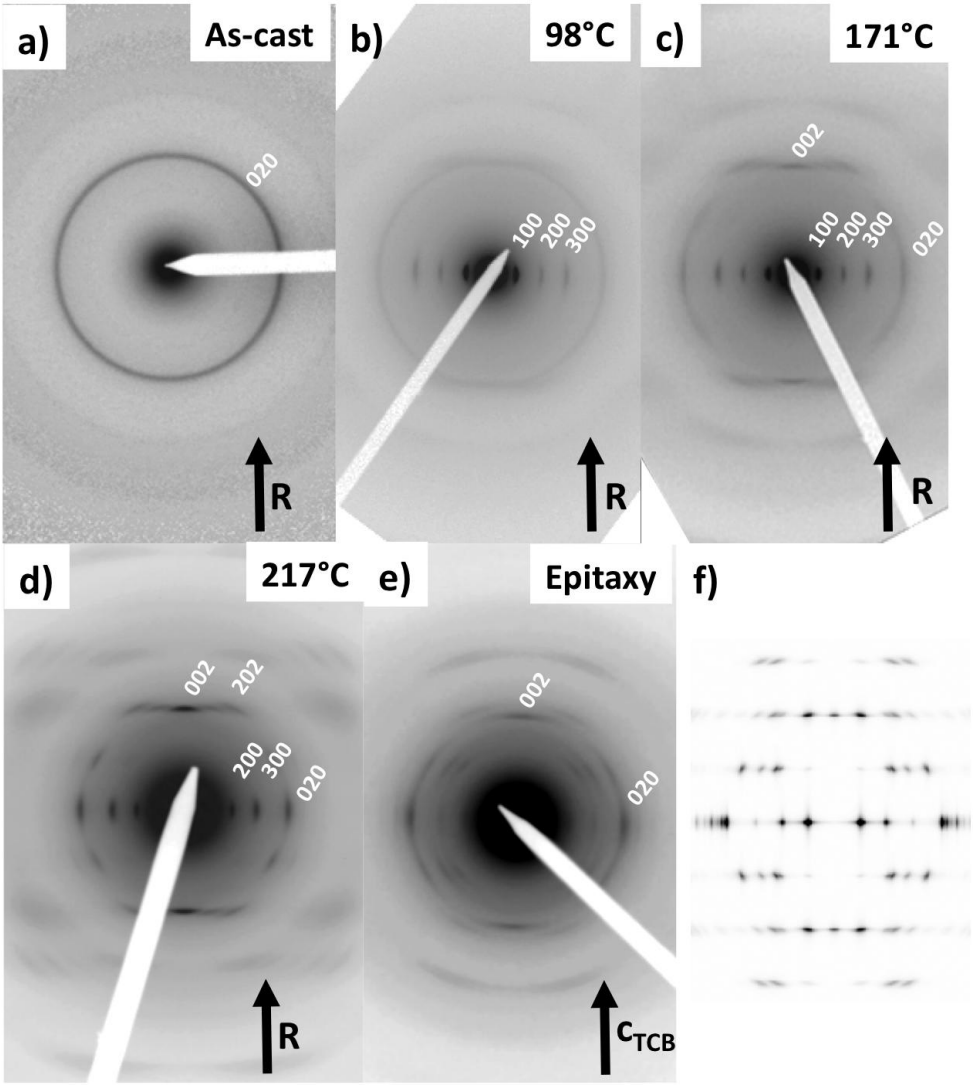

Figure 3. Evolution of the ED diffraction patterns in rubbed P3HT films as a function of the rubbing temperature T_R. For each ED pattern, the direction of rubbing (R) is indicated by an arrow. For comparison, (e) shows the ED pattern of an oriented P3HT film prepared by directional epitaxial crystallization in TCB. The direction of the $\mathbf{c_{TCB}}$ axis of the substrate is indicated by an arrow. (f) is a calculated fiber pattern using the structure of form I obtained from epitaxied low-M_w P3HT. [37]

d) HR-TEM: evaluation of stem lengths in oriented crystals.

BF TEM demonstrates that the total lamellar period (crystalline plus amorphous) scales with the rubbing temperature T_R. Most relevant for charge transport is the size of the crystalline domains relative to the amorphous interlamellar zones. The average length of the P3HT stems in the crystals, l_c can be extracted from HR-TEM images showing crystalline domains in *face-on* orientation since a strong contrast exists between the electron-dense layers of π-stacked backbones (containing sulfur atoms) and the layers of alkyl side chains.[38,39] Therefore HR-TEM images show typical fringed patterns with a 1.65 nm period (corresponding to a_{P3HT}). This methodology was applied here in the case of crystalline domains formed in high-T rubbed films. Figure 4 shows some representative low dose HR-TEM images and the extracted histograms of stem lengths (l_c) for P3HT films rubbed at 144°C (a), 171°C (b) and 217°C (c). The statistical analysis shows that the average value of l_c does indeed increase with the rubbing temperature. Importantly, a four-fold increase of l_c is observed between 144°C and 217°C, corresponding to stems of 9 to 36 thiophene units in average, respectively. This result is in line with the ED observations showing enhanced diffraction at increased T_R and a progressive increase of intensity and sharpening of the 0 0 2 reflection in the ED patterns.

Since we know the values of l_c and l for various temperatures, it is possible to extract a crystallinity $\chi_{HRTEM} = l_c/l$. This definition assumes that the crystalline order of the films along the **a** and **b** axes does not substantially change for 144°C≤T_R≤ 217°C. The values given in Table 1 indicate that the crystallinity χ_{HRTEM} is increasing with T_R up to a value of 56% at 217°C. As shown below, the values of χ_{HRTEM} are in close agreement with those obtained from the DSC analysis of the rubbed samples (vide infra).

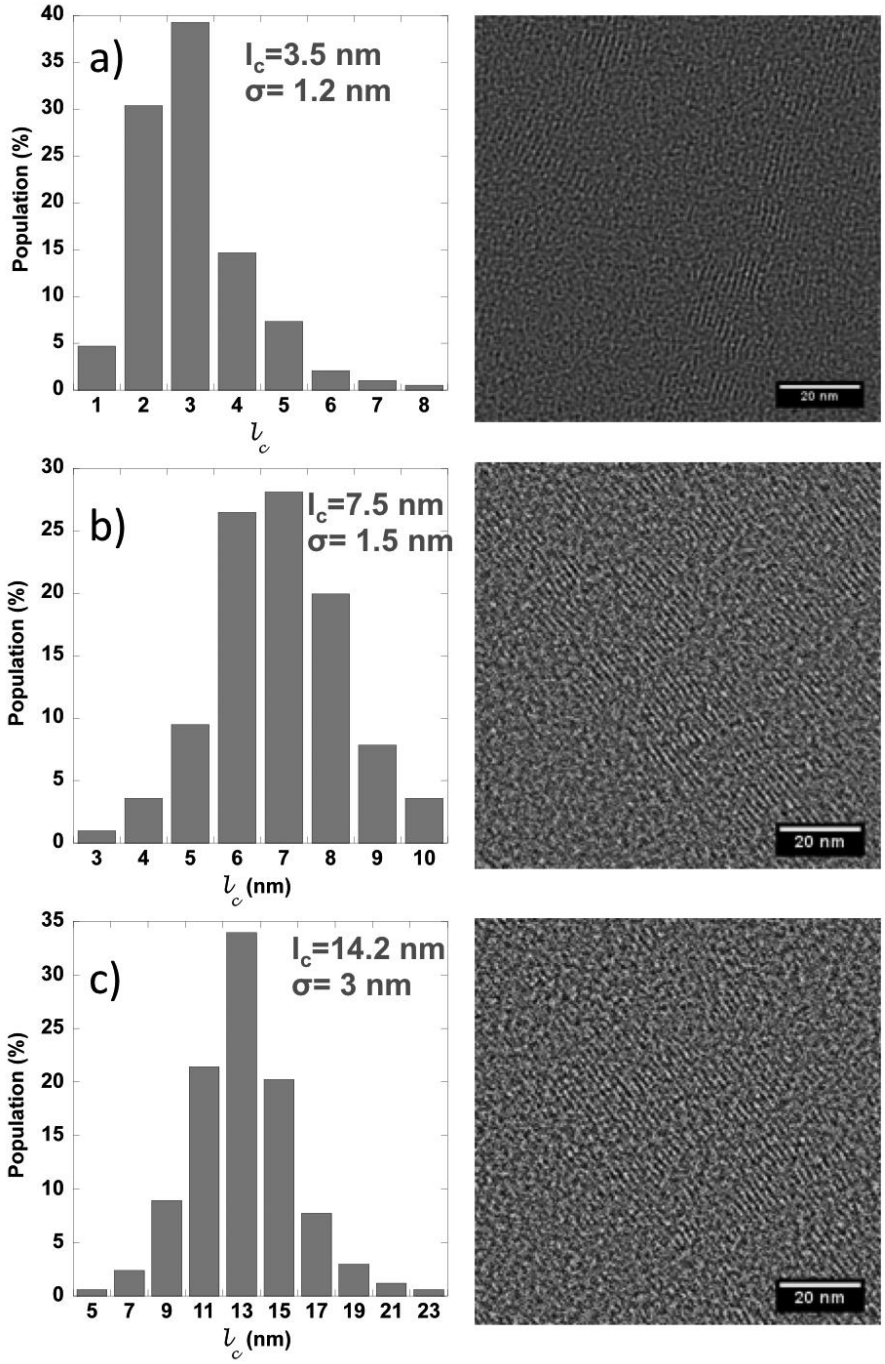

Figure 4. Statistical analysis of the stem length (l_c) extracted from the HR-TEM images of oriented P3HT films prepared by rubbing at different temperatures. a) T_R=144°C, b) T_R=171°C and c) T_R=217°C.

2.2. Differential scanning calorimetry.

Having observed different morphological and structural features in the P3HT films rubbed at different temperatures, we have analyzed the rubbed films by DSC, in particular to follow the variation of crystallinity χ_{DSC} with T_R. To this aim, only the first heating scan was considered as it is characteristic of the structural state of the sample after rubbing (the second heating scans of all rubbed films all looked similar with almost identical melting enthalpies, see Figure S3). Figure 4 illustrates the evolution of the DSC first heating scans as a function of the rubbing temperature T_R. Table 1 collects the melting enthalpies obtained by integration of the DSC signals over the appropriate temperature ranges as well as the melting temperatures at the peak maximum (see experimental section).

Table 1. Structural data on the semi-crystalline structure of high-T rubbed P3HT films. Lamellar periods (*l*) extracted from BF TEM, melting enthalpy ΔH, crystallinity χ_{DSC} and χ_{HRTEM}, average stem length l_c extracted from DSC and TEM.

T_R	*l* (nm)	ΔH (J/g)	χ_{DSC} (%) [a]	l_c (DSC) (nm)	l_c (HR-TEM) (nm)	χ_{HRTEM} (%)
144°C	13 ± 1	8.5 ± 2.5	26± 8	3.3 ±2.0	3.5 ± 1.2	25±17
171°C	16 ± 1.5	11 ± 3	33± 13	5.3 ± 3.0	7.5 ± 1.5	47±15
202°C	20 ± 1.5	16 ± 0.5	49 ± 7	9.7 ± 2.0	-	-
217°C	25 ± 2	22 ± 1	66 ± 9	15.3 ± 3.6	14.2 ± 3.0	56±15

[a] The crystallinity χ_{DSC} is calculated by assuming a melting enthalpy for a perfectly crystalline P3HT sample of 33 J/g following reference 40. l_c (DSC) is extracted from the values of *l* and χ assuming that l_c (DSC)=χl. χ_{HRTEM} is calculated from the ratio l_c/l.

Figure 5 shows clear trends concerning the overall shape, the peak positions and the melting enthalpies in the first heating cycle of P3HT films rubbed at different T_R. For $25°C \leq T_R \leq 144°C$, a first exothermic signal is observed around T=225°C. Its enthalpy is a function of T_R and is most important for T_R=98°C. It is absent in the films rubbed at T_R=25°C and for $T_R \geq 144°C$ i.e. the films that show a lamellar semi-crystalline structure. This exotherm is attributed to so-called cold crystallization of P3HT chains that have been pre-oriented by rubbing. *This implies that there exists a fraction of highly oriented P3HT chains forming a metastable phase that crystallizes upon subsequent annealing during the DSC scan.*

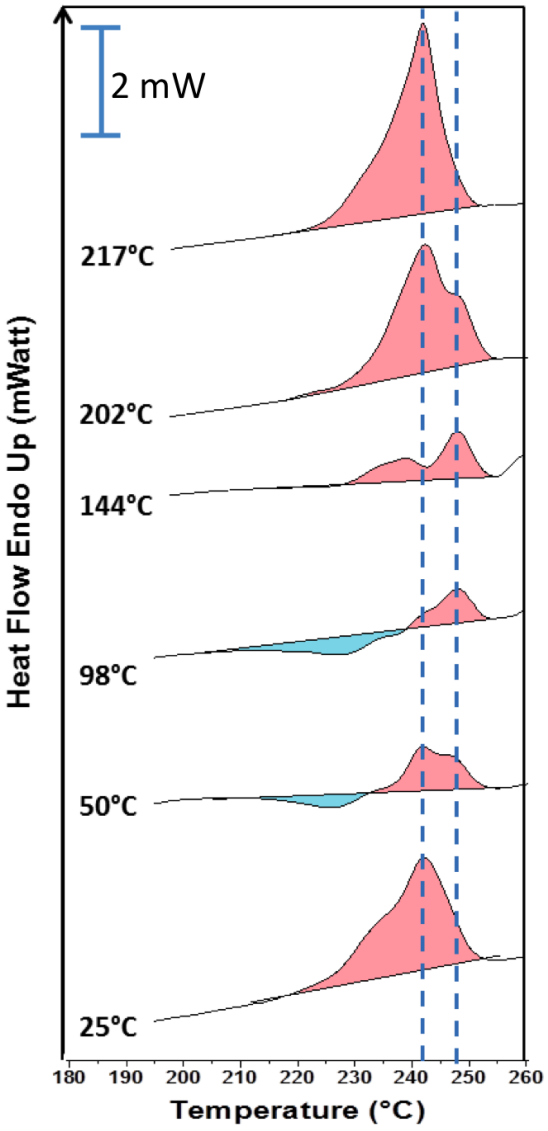

Figure 5. First heating DSC traces for P3HT rubbed films at different rubbing temperatures. For clarity, the DSC traces of the different samples were shifted along the ordinate axis. As a guide to the eye, the exotherm corresponding to the cold crystallization is highlighted in blue and the area of the melting endotherm in pink . The dotted lines highlight the peak positions of two observed melting endotherms at 241 and 248°C.

Following this exotherm, two melting endotherms are observed at T~241°C and 248°C. Their relative enthalpies vary with T_R. The 241°C endotherm first decreases, reaches a minimum for T_R = 98°C and then increases until T_R = 217°C. By contrast, the enthalpy of the 248°C endotherm increases as T_R reaches 144°C and then decreases until it disappears for $T_R \geq 217$°C. Both melting endotherms are accordingly associated to two types of crystalline domains formed under different conditions.

In fact, both the cold crystallization exotherm and the 248°C melting endotherm appear and disappear concomitantly in the heating scans. Since the exotherm is associated to cold crystallization of aligned chains, the 248°C melting endotherm must correspond to the melting of the cold crystallized fraction during the DSC measurement. The higher value of T_m might indicate that cold-crystallized P3HT chains form crystalline domains with more extended chains.

Despite the presence of the exotherm associated with the cold crystallization of rubbed P3HT, the total melting enthalpy ΔH_m was tentatively extracted from the entire endotherm peak (in pink). As seen in Figure 6, a rather clear evolution of ΔH_m is observed with T_R. In the range 25°C – 98°C, ΔH_m decreases to 3 J/g. Then, for $T_R \geq 98$°C, ΔH_m increases with T_R to a maximum value of 22 J/g.

The comparison of the structural information gathered by TEM allows us to rationalize the DSC results and propose the following rationale. Rubbing the films at T_R=25°C leaves the films almost unaffected structurally without any alignment of the chains. Therefore the characteristics of the melting endotherm are similar to that of the non rubbed films in terms of peak position (endotherm at 241°C) and enthalpy.

For 98°C≤T_R≤144°C, the film's structure consists of a fraction of non oriented crystalline phase (evidenced by the 0 2 0 Scherrer ring in the ED pattern) and an oriented "smectic-like" phase with face-on oriented domains. In the smectic-like phase, polythiophene backbones are π-stacked into layers surrounded by layers of more or less disordered side chains. Inside a layer of π-stacked chains, no translational order along the chain direction is observed between successive chains as inferred from the absence of the 0 0 2 reflection.[25] The non oriented P3HT crystalline phase gives rise to the melting endotherm at 241°C whereas both the exotherm due to cold crystallization and the melting endotherm at 248°C are attributed to the aligned smectic-like phase. The cold crystallization evidenced for films rubbed at 98°C≤T_R≤171°C is therefore attributed to the crystallization of the aligned P3HT chains of the smectic-like phase during the heating scan. A second important result concerns the presence of a melting endotherm close to 248°C in the films rubbed at T_R≤202°C. This endotherm might be linked with a fraction of highly oriented and possibly extended P3HT chains of the aligned smectic phase. In contrast to the folded chains found in the semi-crystalline phase with 3D order for T_R≥144°C, the crystalline domains formed upon cold crystallization of the aligned smectic-like phase may involve a larger fraction of extended chains responsible for a higher melting temperature.

When T_R ≥144°C, the periodic lamellar structure characteristic of semi-crystalline P3HT is formed. The size of the crystalline domains and of the total lamellar period *l* (crystalline + amorphous) increases with T_R as does the melting enthalpy.

The melting endotherm of rubbed P3HT films with a semi-crystalline morphology is little affected by the increased lamellar periodicity for T_R≥144°C. Only a slight shift of T_m is observed between 238.5 °C and 241.5°C for T_R=144°C and 217°C, respectively. This

situation is similar to that observed for powders of poly(3-octylthiophene) (P3OT) by Causin et al.[41] For P3OT films, a very small 2°C shift of the melting temperature T_m was evidenced when T_C changes from 140°C to 170°C.

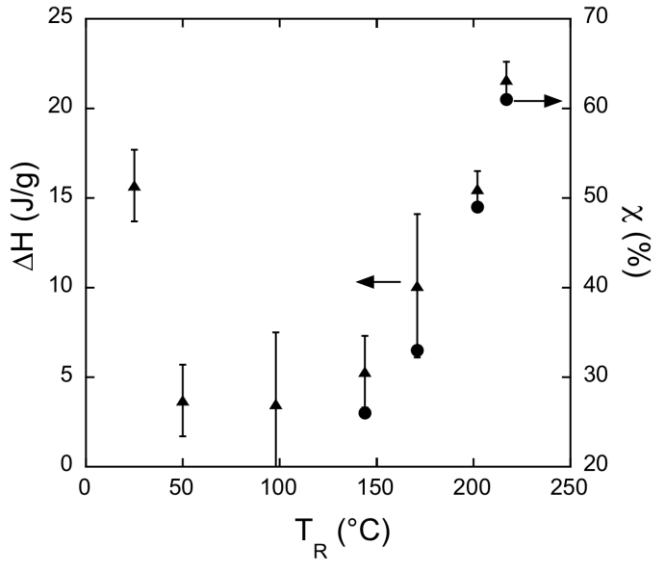

Figure 6. Evolution of the melting enthalpy ΔH_m (full triangles) extracted from the 1st heating scan in the DSC of rubbed P3HT films and crystallinity χ (full circles) as a function of the rubbing temperature T_R.

The most interesting finding of the DSC result is the observed increase in melting enthalpy with T_R, especially for the films showing a regular lamellar periodicity l ($T_R \geq 144$°C). Previous studies by Thurn Albrecht et al. have established a melting enthalpy for an infinite P3HT crystal of 33 J/g. [40] Accordingly, it is possible to determine an apparent crystallinity χ_{DSC} and hence the average stem length in the crystalline regions l_c defined as $l_c(DSC)=\chi_{DSC} l$. Table 1 collects the values of χ_{DSC} and the average crystal size along the chain direction $l_c(DSC)$ versus T_R. Interestingly, the crystal size l_c increases substantially between 144°C and 217°C from 3 nm to 15 nm whereas the

crystallinity χ varies between 26 % and 66 %, respectively. Most interestingly, the average stem length l_c(DSC) is in close agreement with the statistical stem length obtained from HR-TEM measurements, within experimental errors. This supports the total crystallinity values extracted from the DSC measurements on the films rubbed at various temperatures. The maximum crystallinity values obtained at 217°C are also in line with the X-ray values of 68-80% reported by Thurn-Albrecht and coworkers for powdered samples.[40] This result demonstrates that high-T rubbing allows to precisely tune the crystallinity of the P3HT samples in a reproducible way. The control of the rubbing temperature T_R gives therefore a handle on the crystal size along the chain direction l_c and on the total crystallinity χ. We will now discuss the impact of crystal size on optical and charge transport properties in the oriented P3HT films.

2.3. Correlation between l_c and excitonic band width W.

The optical absorption of P3HT films contains physical information on the polymer chain conformation. A random coiled P3HT chain in solution absorbs at 460 nm whereas planarization of the chains upon crystallization transforms the spectrum to a well-defined vibronic progression. The relative weight of the vibronic components A_{0-0} and A_{0-1} is a measure of the level of order, as inferred from studies on solvent cast films and crystallization of P3HT in solution. Large A_{0-0}/A_{0-1}ratios are observed in highly crystalline films of P3HT prepared from high boiling point solvents such as chlorobenzene, mesitylene or isodurene.[42,43]

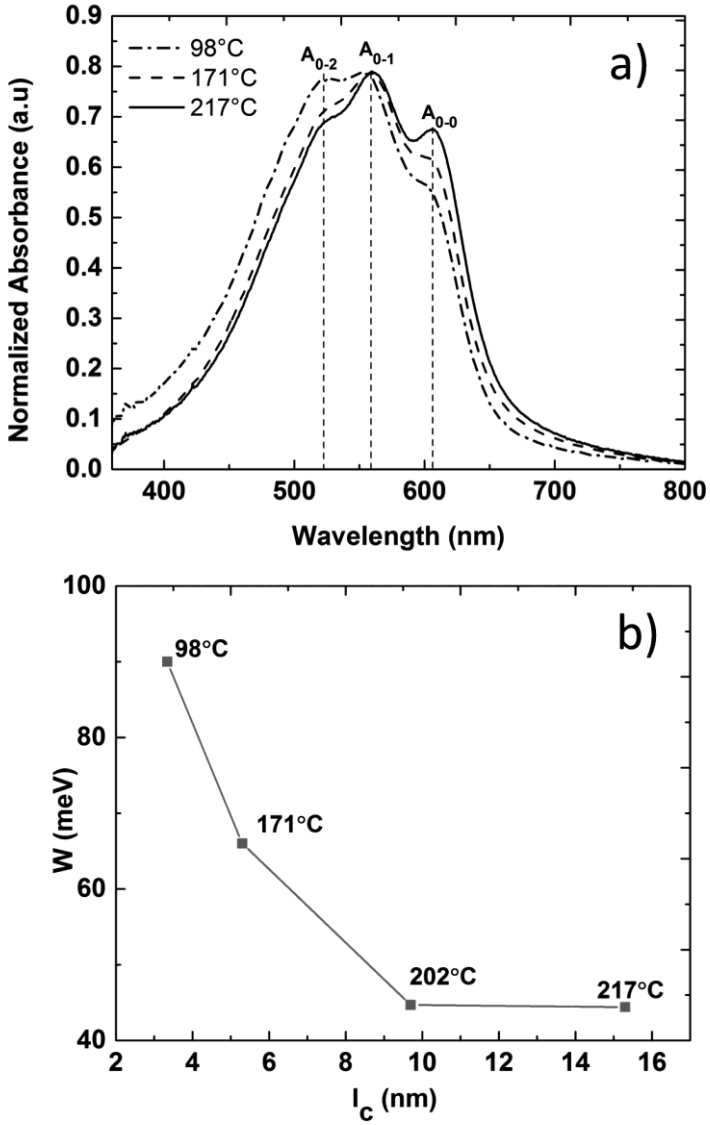

Figure 7. a) Polarized UV-vis absorption spectra of oriented P3HT films prepared by high-T rubbing at various temperatures. The spectra correspond to the incident polarization parallel to the rubbing direction R and are normalized with respect to the absorbance of the 0-1 component of the vibronic structure. b) Evolution of the exciton band width W as a function of the average stem length of crystalline domains l_c.

Although the importance of the solvent used for the processing is known, no correlation between the crystalline features of the films e.g. crystal dimensions and the optical properties has been established so far. As shown in the previous section, high-T

rubbing gives a handle to control the size of the crystalline domains along the chain direction, hence, to investigate possible correlations with optical properties such as the exciton band with W extracted from the ratio $A_{0\text{-}0}$ / $A_{0\text{-}1}$.

Figure 7 depicts the evolution of the UV-Vis absorption spectrum with rubbing temperature (polarization parallel to the rubbing direction R). All spectra exhibit the characteristic vibronic structure with three dominant contributions associated to the 0-0, 0-1 and 0-2 transitions centered at 610 nm, 555 nm and 525 nm, respectively. For T_R=98°C, both the 0-2 and 0-1 components are dominant whereas the 0-0 contribution is seen as a shoulder. Such a spectrum is similar to that observed in strain-aligned P3HT films.[13] The low intensity of the 0-0 component is in line with the limited crystallinity evidenced by TEM. Increasing T_R results in the strong increases of the ratio $A_{0\text{-}0}/A_{0\text{-}1}$ and a decrease of $A_{0\text{-}2}/A_{0\text{-}1}$. For T_R=217°C, the $A_{0\text{-}0}$ component is very well defined, as for highly crystalline films of P3HT prepared by solvent vapor annealing.[14] The overall trend observed for the absorption spectrum follows the observed structural evolution seen by TEM: increasing T_R above 171°C results in a remarkable increase in overall crystallinity of the rubbed films that show a periodic lamellar structure characteristic of a semi-crystalline polymer.

Referring to the weak H-aggregate model of Spano et al.,[44] it is possible to extract information on the local intrachain order from the UV-Vis spectra. Indeed, Spano et al. showed that the free exciton band width W for weak H-aggregates is related to the ratio $A_{0\text{-}0}/A_{0\text{-}1}$ following the equation :

$$\frac{A_{0-0}}{A_{0-1}} = \left(\frac{1 - 0.24\,W / E_p}{1 + 0.073\,W / E_p} \right)^2 \qquad \text{(Eq. 1)}$$

where E_p is the energy of the main intramolecular transition (corresponding to a symmetric C=C stretch).[42] Following the work by Clark et al., a decrease in W is associated to an increase in the effective conjugation length. In the present case, we observe that W decreases with increasing T_R from 93 to a plateau value of 44 meV for T_R=217°C. This value is remarkably small for such a high-M_w P3HT sample processed in the solid-state i.e. in absence of solvent. It is similar to that observed in P3HT spherulites grown by SVA.[16] It is therefore the fingerprint of high crystallinity in the films prepared at 217°C.

The excitonic coupling between planarized chain segments should decrease with the increasing length of the segments. Calculations of the excitonic coupling dependence with the extension of the planarized chain segments has been performed by Gierschner et al. and Beljonne et al. for various conjugated polymers such as polythiophene.[44,45] Since the size of the crystalline stems can be controlled in the rubbed P3HT films, we have a mean to probe how the limited crystal size impacts the value of W. Interestingly, our HRTEM results give a direct measure of the average planarized chain segments that can be approximated by l_c. Figure 7.b depicts the variation of W *versus* average stem length l_c in the crystals. The fact that W first decreases with T_R indicates that the conjugation length is limited by the average stem length l_c in the crystalline domains. However, for T_R=202°C, W reaches a plateau at 44 meV. Therefore, the value of l_c at ~202°C is an indirect measure of the maximum conjugation length achieved in semi-crystalline P3HT films. This conjugation length is close to 10 nm and corresponds to 25 thiophene units. It must be stressed that this value is in good agreement with the conjugation length of the 40-60 monomer predicted by implementing Zerner's Intermediate Neglect of Differential Orbital method on P3HT films grown from

isodurene solution (W=20 meV).[45,46] The lower value of W achieved in films cast from isodurene is related to the fact that, P3HT crystals grown from solution form fibrils with neatly folded chains and without extended amorphous interlamellar zones as observed in our rubbed films. In average, the width of P3HT fibrils, corresponding to l_c, is in the range 18 – 20 nm i.e. larger than the maximum value of l_c observed in the rubbed films (16 nm).[47]

2.4. Charge transport anisotropy.

To evaluate the impact of the controlled crystallinity and in-plane alignment on the charge transport properties, bottom-gate bottom-contact OFETs were fabricated using the rubbed P3HT films. It is worth mentioning that we did not aim at optimizing the transistor performances but mainly at correlating the structure, crystallinity and morphology of the films with charge transport properties observed in bottom-gate bottom-contact transistors. We probed the charge transport in both parallel (//) and perpendicular ($\perp$) directions to the source-drain contacts. Some representative output and transfer curves of the rubbed samples in both directions are shown in Figure S4.

The output characteristics show good saturation behavior and "negligible" non linear characteristics in the low drain (V_{DS}) voltage region. The field-effect mobilities were extracted from the transfer characteristics in the saturation regime by assuming a gate voltage independent transport and a negligible contact resistance (see Figure S4). The evolution of the hole mobilities in both parallel ($\mu_{//}$) and perpendicular directions ($\mu_{\perp}$) as a function of rubbing temperature T_R are shown in Figure 8. Except for the sample that was melt- annealed, all rubbed films exhibit some anisotropy of the charge mobility. The highest anisotropy is observed for the films rubbed at 50°C whereas the lowest anisotropy is observed for the sample prepared at 217°C. No direct correlation

between the 3D order parameter extracted from the polarized UV-Vis absorption and the observed charge transport anisotropy could be evidenced. The only correlation might be that the decrease in orientation for $T_R \geq 171°C$ coincides with a corresponding decrease in the mobility anisotropy.

Surprisingly, the hole mobility in the direction parallel to **R** is not showing a strong variation for $T_R \leq 171°C$. All values of $\mu_{//}$ lie in the range 2-4 $x10^{-3}$ $cm^2/V{\cdot}s$. Also, the value of $\mu_{//}$ is not found to surpass that of the as doctor bladed films. For $T_R > 171°C$, $\mu_{//}$ decreases slightly and increases again after melting (240°C). Regarding hole transport in the direction perpendicular to the rubbing, the results in Figure 8 show a stronger impact of T_R. For T_R in the range 50°C-144°C, $\mu_\perp$ shows first an increase. Then, for $144°C \leq T_R \leq 198°C$ $\mu_\perp$ tends to level at a value of 5 $x10^{-4}$ $cm^2/V{\cdot}s$ and finally, as T_R approached the melting temperature, it is increasing again until it reaches a value close to $\mu_{//}$ (as expected for an isotropic system after melting).

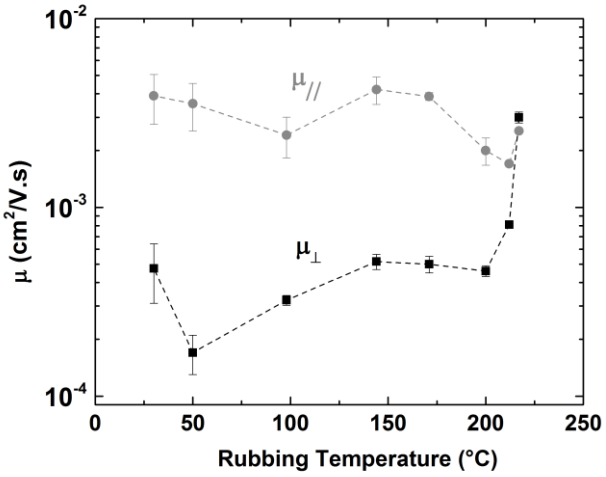

Figure 8. a) Evolution of hole mobility in bottom-gate bottom-contact OFETs made of oriented P3HT films prepared by mechanical rubbing at different temperatures. The

mobility is measured in // ($\mu_{//}$) and $\perp$ ($\mu_{\perp}$) orientations with respect to the rubbing direction R.

2.5. Discussion.

In the following, the observed variations in charge mobilities are analyzed as a function of structural modifications evidenced by TEM (see Figure 9). For $144°C \leq T_R \leq 217°C$ where the semi-crystalline lamellar structure is progressively developing with an increase in lamellar thickness and overall crystallinity, $\mu_{//}$ tends to decrease slightly whereas $\mu_{\perp}$ is increasing. This result indicates that the increase of both crystallinity and crystal size l_c does not translate in an improved charge transport along the rubbing **R** but rather along the perpendicular direction. This result might be understood by considering the detrimental role of extended amorphous interlamellar zones on the macroscopic charge transport in the direction parallel to the rubbing. Amorphous interlamellar zones contain chain ends, chain folds and tie-chains that bridge successive lamellae through the amorphous zones. As noted earlier by Kline et al., there is a need for tie chains or tie crystallites to bridge successive P3HT crystals to enhance macroscopic transport.[7] To evaluate the role of tie chains, it is instructive to compare the average contour length of the P3HT chains, L, and the lamellar periodicity in the samples. In the sample used herein, L ~ 60-70 nm which is far superior to the largest value of the lamellar periodicity observed in the rubbed films (29 nm). Therefore, for all rubbed samples showing a semi-crystalline morphology, some P3HT chains do necessarily bridge successive lamellae through the amorphous zones (see Figure 9). Second, when the applied electric field E is parallel to R, charges must channel through amorphous domains that systematically limit transport in this direction. Our UV-Vis absorption results suggest that the amorphous zones are possibly enriched in

low-M_w fractions of P3HT that do not crystallize. The GPC trace further support this hypothesis since small polymer chain fractions can be seen at high retention time (Figure S2). It is known that the charge mobilities of such low-M_w fractions are usually quite low (~10^{-6} $cm^2/V{\cdot}s$ for 3kDa P3HT).[6] Accordingly, the regular alternation of amorphous zones and crystalline domains must necessarily be detrimental for the large scale transport in the direction parallel to R. Despite the fact that in average, P3HT chains can bridge successive crystalline lamellae through amorphous zones in the direction parallel to R, the twisted conformation of the polythiophene backbone is highly unfavorable for charge transport between crystalline areas. *This implies that the existence of only tie chains is not sufficient to efficiently channel the charges between crystalline domains, most important would be a planar conformation of such tie chains as could be observed in tie-crystallites*. [38,39]

The situation in the direction perpendicular to the rubbing is different. ED clearly shows that the proportion of edge-on crystals increases with T_R. Accordingly, $\mu_\perp$ should progressively change from a value characteristic of transport along the alkyl side chains at low T_R to a value typical of transport along the π-stacking direction at high T_R, which explains in part the evolution of $\mu_\perp$ with T_R. This situation is analogous to that of rubbed PBTTT showing a similar change in charge transport anisotropy when the dominant contact plane changes from mainly *face-on* to *edge-on*.[27] The progressive increase of $\mu_\perp$ with T_R may have a second origin. The BF-TEM images show a high continuity of crystalline lamellae in the direction perpendicular to R, which should therefore be favorable for charge transport along that direction. In other words, whereas amorphous interlamellar zones interrupt transport in the direction parallel to R at a small length scale of max. 15-20 nm, the continuity of the crystalline domains in the direction

perpendicular to R over larger distances (up to 100 nm at 217°C) should ensure a more efficient transport. Therefore, the increase in film crystallinity with T_R explains in part the increase of $\mu_{\perp}$. Conversely, it is the highly regular semi-crystalline lamellar morphology that hampers charge transport in the direction of the rubbing. It is worth to note that this situation is different from the case of spin-coated or cast films from solution that consist of solution grown nanofibrilar crystals that do not have extended amorphous zones around their crystalline cores.[47] Moreover, it must also be reminded that charge transport in rubbed polymer layers measured in bottom-gate bottom-contact configuration is always found to be lower as compared to that measured in top-gate and bottom-contact geometry.[48] As a test, we have probed also the transport on the top surface of a rubbed film for T_R= 171°C. To this aim, the rubbed P3HT film was prepared on NaPSS and floated on distilled water and deposited on an OFET substrate (patterned SiO_2 BG-BC substrates) in such a way that the polymer/air interface would now face the SiO_2 substrate. Values of $\mu_{//}$=6.6 x10^{-2} $cm^2/V{\cdot}s$ and $\mu_{\perp}$=1.8 x10^{-2} $cm^2/V{\cdot}s$ were obtained (see Figure S5). This result shows that transport at the SiO_2/P3HT and Air/P3HT interfaces are different. A possible reason for this result is that the structure of the films are different at both interfaces, especially in terms of crystallinity. For spin coated films, it is well known that the structure of the P3HT film at the buried interface with the substrate can be significantly different from that in the bulk.[49,50] It can be anticipated that the P3HT chains located at the SiO_2 interface may have more difficulties to align and crystallize than those chains located at the film interface directly in contact with the rubbing cloth. Moreover, it must also be recalled that the charge mobilities of rubbed PBTTT and p(NDI2OD-T2) films prior to annealing were always rather low because of the structural damage in the films caused upon rubbing.[23,28] Usually, in all these systems, post-rubbing annealing was necessary to induce a substantial increase of

the charge mobilities by 1-2 orders of magnitude as compared to the as-rubbed films. In the case of P3HT, it is observed that post-rubbing annealing at temperatures above 100°C induces a substantial loss of in-plane orientation, which was not observed for the more rigid PBTTT or p(NDI2OD-T2).

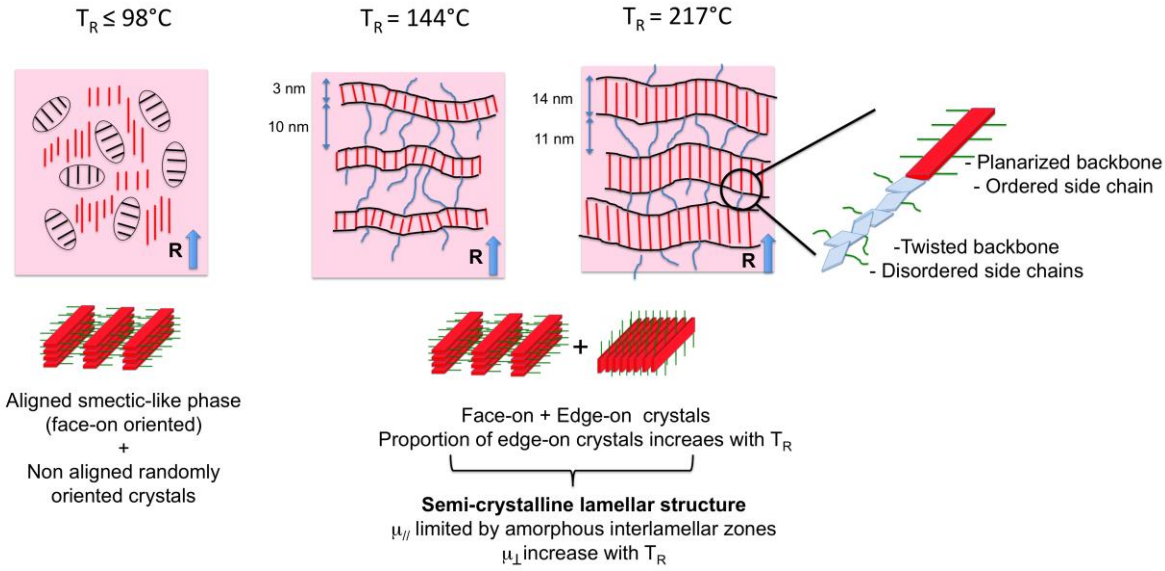

Figure 9. Schematic illustration of the structural evolution in rubbed P3HT films as a function of the rubbing temperature T_R and impact on charge transport. For clarity, only the crystalline domains are represented, the amorphous areas are highlighted in light pink. A certain number of tie chains linking successive crystalline domains as well as chain ends are shown in blue within the amorphous zones.

3. Conclusions.

High-T rubbing is a unique method that allows to fine tune the lamellar period in semi-crystalline films of SCPs such as P3HT by adjusting the rubbing temperature T_R. This is possible since the nucleation of crystalline domains, often difficult for such rigid polymers, is induced by mechanical rubbing at a sufficiently high temperature that

allows P3HT to crystallize and form a regular lamellar semi-crystalline morphology. The periodicity of the lamellar semi-crystalline structure, *l*, scales with the rubbing temperature such as $l^{-1} \propto (T_m^0 - T_R)$ with T_m^0=301°C. A rather clear correlation is observed between the exciton band width W and the average crystal size l_c since l_c is limiting the conjugation length in the films (extent of planarized chain segments). Regarding charge transport, the anisotropy of charge mobility $(\mu_{//})/(\mu_{\perp})$ is shown to decrease with T_R. The mobility parallel to the chains, $\mu_{//}$, does not substantially increase with the overall crystallinity χ. This relative constancy is explained by the presence of amorphous interlamellar zones that hamper charge transport along the rubbing direction whatever the value of T_R in the range 144°C-217°C. The existence of only tie chains linking successive crystalline domains seems not sufficient to efficiently channel the charges through amorphous interlamellar zones. In strong contrast, the hole mobility perpendicular to the chain direction, $\mu_{\perp}$, is more clearly correlated to both the crystallinity in the samples and the proportion of edge-on crystals in the films. Preliminary results were obtained on other polyalkylthiophenes e.g. poly(3-butylthiophene) as well as low bandgap polymers such as (F-PCPDTBT). They indicate that the methodology followed herein is very general and can be used to elaborate thin films with periodic semi-crystalline structures with high crystallinity, tunable crystal dimensions and orientation. These aspects are essential to clarify the processing-structure-property *nexus* of conjugated semi-crystalline polymers.

4. Experimental section.

a. Materials and sample preparation.

The poly(3-hexylthiophene) (P3HT) is purchased from Rieke (RMI-001E, batch number BS21-44). This batch has a regioregularity of 97%, M_w=48 kg/mol and PDI=1.64 (see Figure S2 for the GPC analysis). For TEM and UV-vis studies, all P3HT films are prepared by doctor blading a 5wt% solution in *ortho*-dichlorobenzene (*o*-DCB) on clean glass slides (Roth) maintained at 170°C. Cleaning of the glass substrates is described in the literature.[51]

For DSC studies, the clean glass slides are first coated with a thin film of 10 wt % NaPSS aqueous solution (poly(sodium 4-styrenesulfonate) from Sigma Aldrich, average M_w ~ 10^6 g/mol) by spin-coating (3000 rpm for 45 s and 200 rpm/s). The P3HT films are then doctor-bladed on top of the NaPSS sacrificial layer using a 10 wt% solution in *o*-DCB and then rubbed. The rubbed P3HT films are slowly immersed in water to dissolve NaPSS. The floated P3HT films are collected and dried overnight under primary vacuum. Finally several rubbed films (total weight of 5-6 mg) are fit inside inox pans. Mechanical rubbing of P3HT films was performed following the methodology described in our previous work.[25,27,28] In brief, a microfiber cloth is applied at a pressure of 2.3 – 3.0 bar on the P3HT films. The so-called rubbing length is fixed at ca. 50 cm, and three rubbing cycles are used. To avoid chemical degradation of the films in ambient during high temperature rubbing, the rubbing was performed in a glove box (Plas Labs, Inc.) with $p(O_2) < 0.01\%$.

Prior to rubbing, the film was allowed to stabilize for 1-2 min at the desired temperature. A careful calibration of the surface temperature of both silicon substrates and glass substrates on the rubbing machine was performed with a platinum RTD resistance in order to determine possible biases between the setting temperature and the real temperature on the sample surface during rubbing. All values of T_R given hereafter correspond to the real temperatures measured on the samples.

b. Sample characterization.

UV-Vis spectroscopy: Polarized UV-vis absorption spectroscopy was performed using a Varian Carry 5000 UV-VIS-NIR spectrometer with polarized incident light.

TEM analysis: A thin amorphous carbon film is evaporated on the P3HT rubbed films using an Auto 306 evaporator (Edwards). Then, samples are removed from the glass substrate by floating the films in a 5 wt% aqueous HF solution and recovered on TEM copper grids. TEM was performed in bright field, high resolution and diffraction modes using a CM12 Philips microscope equipped with a MVIII (Soft Imaging System) Charge Coupled Device camera. Specific conditions for HR-TEM and low dose diffraction are given elsewhere.[36, 37]

DSC measurements: Differential scanning calorimetry (DSC) analyses were performed under argon on a DSC manufactured by Setaram. The heating/cooling rates are set to 15°C/min. The melting enthalpies were extracted from the 1st heating cycle using the Pyris software (11.0 version). The error bars on the melting enthalpies are estimated from the contribution of the cold crystallization enthalpy since it generates an additional contribution to the true melting enthalpy of the rubbed films.

OFET characterization: Bottom-gate bottom-contact field-effect transistors (FETs) were elaborated on pre-patterned test structures (Fraunhofer) whose source and drain contacts were composed of a 30 nm thick gold layer on top of a 10 nm thick Indium Tin Oxide (ITO) layer. A 230 nm thick silicon oxide was used as gate dielectric and n-doped silicon crystal as gate electrode. The channel length and channel width are L=20 µm and W= 10 mm,

respectively. These electrode patterns were oriented along two directions on the substrates at 90° relative orientation so that charge transport could be measured both parallel and perpendicular to the rubbing direction. The transistor substrates were cleaned by sonication in acetone and isopropanol at 45°C for 15 min in each solvent. After drying under nitrogen, the substrates were subsequently exposed to an ultra-violet ozone atmosphere for 15 min. No surface functionalization of the SiO_2 with OTS or HMDS was performed because it was found to alter the efficiency of the rubbing process (films are partly removed from the modified SiO_2 substrates upon rubbing). Polymer films of ~ 50 nm thickness were spin-coated from 5wt% solutions in *o*-DCB (1250 rpm for 120 s and then 2000 rpm for 60 s). The polymer solutions were prepared by dissolution at 80°C for 4 hrs under continuous stirring. After deposition, the samples were left under vacuum (<10^{-6} mbar) overnight to remove residual solvent traces. All polymer solutions and films were prepared in a nitrogen atmosphere.

After rubbing of the films, the electronic characterization of the OFETs was carried out in a nitrogen atmosphere using a Keithley semiconductor parametric test system. The field-effect mobilities (μ_{FET}) were determined from the current-voltage transfer characteristics in the saturation regime using the following equation[52]:

$$\mu_{sat} = \left(\frac{\partial \sqrt{I_{Dsat}}}{\partial V_G} \right)^2 \cdot \frac{2L}{WC_i} \quad (1)$$

where I_{Dsat} is the source-drain current, V_g is the gate voltage, and C_i is the capacitance per unit area of the gate dielectric.

The mobility values were measured for both the saturation and the linear regimes. Both mobilities showed the same trends as a function of the rubbing temperature. For the low

rubbing temperature (below 100°C) devices, we have observed an important contact resistance. In such case, charge transport was probed for several channel lengths (20, 10 and 5 µm) and corrected value of mobilities were extracted following the procedures described in the literature.[52] As contact resistance has more impact at low voltage and might affect the extraction of hole mobilities, only hole mobilities in saturation regime are discussed herein. 2-3 devices were used to measure mobilities and charge anisotropy for each rubbing temperature. The reported values of mobilities are the mean arithmetic values and the error bars are calculated as the standard deviations of the obtained values.

Acknowledgments.

Bernard Lotz is gratefully acknowledged for fruitful discussions and careful reading of the manuscript. C. Blanck and M. Schmutz are gratefully acknowledged for technical support in TEM. Chheng Ngov is acknowledged for performing the GPC analysis and C. Saettel for DSC measurements. We are extremely gratefull to the MaCEPV team at ICUBE (N. Zimmermann, P. Lévèque and T. Heiser) for technical support in charge transport measurements, privileged access to the glove box plateform and fruitfull discussions on charge transport measurements. Support from the IRTG Soft Matter and the European community (Rhin Solar Interreg project C25), the Université de Strasbourg, the Investissements d'avenir (IDEX) and the Fédération de recherche Matériaux et Nanosciences Alsace are gratefully acknowledged.

References.

1) a) H. Sirringhaus, J. P. Brown, R. H. Friend, M. M. Nielsen, K. Bechgaard, B. M. W. Langeveld-Voss, A. J. H. Spiering, R. A. J. Janssen, E. W. Meijer, P. Herwig and D. M. de Leeuw, *Nature* **1999**, *401*, 685. b) R. Noriega, J. Rivnay, K. Vandewal, F. P. V. Koch, N. Stingelin, P. Smith, M. F. Toney and A. Salleo *Nat. Mater* **2013**, *12*, 1038.

2) a) C. Poelking, K. Daoulas, A. Troisi and D. Andrienko *Adv. Polym. Sci.* **2014**, *265*, 139. b) Y.-K. Lan and C.–I. Huang, *J. Phys. Chem. B* **2009**, *113*, 14555.

3) a) D. Venkateshvaran, M. Nikolka, A. Sadhanala, V. Lemaur, M. Zelazny, M. Kepa, M. Hurhangee, A. J. Kronemeijer, V. Pecunia, I. Nasrallah, I. Romanov, K. Broch, I. McCulloch, D. Emin, Y. Olivier, J. Cornil, D. Beljonne and H. Sirringhaus *Nature*, **2014**, *515*, 384. b) K. Do, D. M. Huang, R. Faller and A. J. Moulé *Phys. Chem. Chem. Phys.* **2010**, *12*, 14735.

4) M. Brinkmann and P. Rannou *Macromolecule*s, **2009**, *42*, 1125.

5) M. Brinkmann and J.-C. Wittmann, *Adv. Mat.***2006**, *18*, 860.

6) P. Pingel, A. Zen, R. D. Abellon, F. C. Grozema, L. D. A. Siebbeles and D. Neher *Adv. Funct. Mat.* **2010**, *20*, 2286.

7) R. J. Kline, M. D. McGehee, E. N. Kadnikova, J. Liu, J. M. J. Fréchet and M. F. Toney, *Macromolecules* **2005**, *38*, 3312.

8) E. J. W. Crossland, K. Tremel, F. Fischer, K. Rahimi, G. Reiter, U. Steiner and S. Ludwigs *Adv. Mater.***2012**, 24, 839.

9) L. H. Jimison, M. F. Toney, I. McCulloch, M. Heeney and A. Salleo *Adv. Mat.* **2009**, *21*, 1568.

10) M. Aryal, K. Trivedi, W. Hu *ACS Nano*, **2009**, 3, 3085.

11) a) M. Brinkmann, C. Contal, N. Kayunkid, T. Djuriç and R. Resel *Macromolecules* **2010**, *43*, 7604 ; b) M. Brinkmann *Macromolecules* **2007**, *40*, 7532 ; c) M. Brinkmann, N. Charoenthai, R. Traiphol, P. Piyakulawat, J. Wlosnewski and U. Asawapirom *Macromolecules* **2009,** *42*, 8298.

12) D. M. DeLongchamp, R. J. Kline, Y. Jung, D. S. Germack, E. K. Line, A. Moad, J. L. Richter, M. F. Toney, M. Heeney and I. McCulloch *ACS Nano* **2009**, *3*, 780.

13) B. O'Connor, R. J. Kline, B. R. Conrad, J. L. Richter, D. Gundlach, M. F. Toney and D. M. DeLongchamp, *Adv. Funct. Mat.* **2011**, 21, 3697.

14) F. S. U. Fischer, K. Tremel, M. Sommer, E. J. W. Crossland and S. Ludwigs *Nanoscale* **2012**, *4*, 2138.

15) H. R. Tseng, L. Ying, L.; B. B. Y. Hsu; L. A. Perez, C. J. Takacs, G. C. Bazan and A. J. Heeger *Nano Lett.* **2012**, *12*, 6353.

16) E. J. W. Crossland, K. Tremel, F. Fischer, K. Rahimi, G. Reiter, U. Steiner .and S. Ludwigs *Adv. Mat.* **2012**, *24*, 839.

17) L. Bu, E. Pentzer, F. A. Bockel, T. Emrick and R. C. Hayward *ACS Nano* **2012**, *6*, 10924.

18) C. Müller, N. D. Zhigadlo, A. Kumar, M. A. Baklar, J. Karpinski, P. Smith, T. Kreouzis and N. Singelin *Macromolecules* **2011**, *44*, 1221.

19) M. Brinkmann, L. Hartmann, L. Biniek, K. Tremel and N. Kayunkid *Macromol. Rapid. Comm.* **2014**, *35*, 9.

20) H. Zhou and S. Yan *J. Phys.Chem. B* **2011**, *115*, 13449

21) M. Brinkmann, F. Chandezon, C. Julien-Raban and R. P. Pansu *Adv. Funct. Mat.* **2009**, *19*, 2759.

22) L. Liu, J. Zou and L. Zhai *Macromol. Rapid Commun.* **2009**, 30, 1387.

23) M. F. Toney, T. P. Russell, J. A. Logan, H. Kikuchi, J. M. Sands and S. K. Kumar *Nature* **1995**, *374*, 709.

24) H. Heil, T. Finnberg, N. von Malm, R. Schmechel and von H. Seggern *J. Appl. Phys.* **2003**, *93*, 1636.

25) L. Hartmann, K. Tremel, S. Uttiya, E. Crossland, N. Kayunkid, S. Ludwigs, C. Vergnat and M. Brinkmann *Adv. Funct. Mat.* **2011**, *21*, 4047.

26) D. Kajiya, S. Ozawa, T. Koganezawa and K.- I. Saitow *J. Phys. Chem. C* **2015**, *119*, 7987.

27) L. Biniek, N. Leclerc, T. Heiser, R. Bechara and M. Brinkmann *Macromolecules* **2013**, *46*, 4014.

28) L. Biniek, L. S. Poujet, D. Djurado, E. Gonthier, K. Tremel, N. Kayunkid, E. Zaborova, N. Crespo-Monteiro, O. Boyron, N. Leclerc, S. Ludwigs and M. Brinkmann *Macromolecules* **2014**, *47*, 3871.

29) A. Zen, J. Pflaum, S. Hirschmann, W. Zhuang, F. Jaiser, U. Asawapirom, J. P. Rabe, U. Scherf and D. Neher *Adv. Funct. Mat.* **2004**, *14*, 757.

30) S. Samitsu, T. Shimomura, S. Heike, T. Hashizume and K. Ito *Macromolecules*, **2008**, *41*, 8000.

31) A. Keller in : Chain Folded Crystallization of Polymers, from discovery to the present day ; a personalized journey : Sir Charles Frank, OBE, FRS ; 80th brithday tribute ; Chambers, R. G., Enderly, J. D. , Keller, A., Lang, A. R., Steeds, J. W. (Eds.). Bristol, New York, Adam Hilger, pp. 265-306.

32) B. Lotz and J.-C. Wittmann, **2006**. Structure of Polymer Single Crystals. Materials Science and Technology.

33) S. Malik and A. K. Nandi, *J. Polym. Sci. B Polym. Phys.* **2002**, *40*, 2073.

34) F. P. V. Koch, M. Heeney and P. Smith, *J. Am. Chem. Soc.* **2013**, *135*, 13699.

35) C. R. Snyder, R. C. Nieuwendaal, D. DeLongchamp, C. K. Luscombe, P. Sista and S. D. Boyd, *Macromolecules* **2014**, *47*, 3942.

36) The terms “edge-on“ and “face-on“ orientations refer to the orientation of the P3HT backbone with respect to the substrate plane. It must not be confused with the “edge-on“ orientation of crystalline lamellae.

37) N. Kayunkid, S. Uttiya and M. Brinkmann, *Macromolecules* **2010**, 43, 4961.

38) T. S. Salammal, E. Mikayelyan, S. Grigorian, U. Pietsch, N. Koenen, U. Scherf, N. Kayunkid and M. Brinkmann, *Macromolecules* **2012**, *45*, 5575

39) M. Brinkmann and P. Rannou, *Macromolecules* **2009**, *42*, 1125.

40) J. Balko, R. H. Lohwasser, M. Sommer, M. Thelakkat and T. Thurn-Albrecht, *Macromolecules* **2013**, 46, 9642.

41) V. Causin, C. Marega, A. Margio, L. Valentini and J. M. Kenny, *Macromolecules* **2005**, *38*, 409.

42) J. Clark, C. Silva, R. H. Friend and F. C. Spano, *Phys. Rev. Lett.* **2007**, *98*, 206406.

43) J. Clark, J.-F. Chang, F. C. Spano, R. H. Friend and C. Silva, *Appl. Phys. Lett.* **2009**, *94*, 163306.

44) F. C. Spano, *J. Chem. Phys.* **2005**, *122*, 234701.

45) J. Gierschner, Y. S. Huang, B. Van Averbeke, J. Cornil, R. H. Friend and D. Beljonne, *J. Chem. Phys.* **2009**, *130*, 044105.

46) D. Beljonne, J. Cornil, R. Silbey, P. Millie and J.-L. Brédas, *J. Chem. Phys.* **2000**, *112*, 4749.

47) J. Liu, M. Arif, J. Zou, S. I. Khondaker and L. Zhai, *Macromolecules* **2009**, 42, 9390.

48) K. Tremel, F. S. U. Fischer, N. Kayunkid, R. Di Pietro, R. Tchakov, A. Kiriy, D. Neher, S. Ludwigs and M. Brinkmann, *Adv. Energy Mat.* **2014**, 1301659.

49) J. R. Kline, M. D. McGehee and M. F. Toney, *Nature Mat.* **2006**, *5*, 222.

50) W. D. Oosterbaan, J.-C. Bolsée, L. Wang, V. Vrindts, L. J. Lutsen, V. Lemaur, D. Beljonne, C. R. McNeill, L. Thomsen, J. V. Manca and D. J. M. Vanderzande, *Adv. Funct. Mater.* **2014**, *24*, 1994.

51) M. Brinkmann, S. Graff, J.-C. Wittmann, C. Chaumont, F. Nuesch, A. Anver, M. Schaer and L. Zuppiroli, *J. Phys. Chem. B* **2003**, *107*, 10531.

52) a) J. Zaumseil and H. Sirringhaus *Chem. Rev.* **2007**, 107, 1296. b) H. Klauk, *Chem. Soc. Rev.* **2010**, 39, 2643.